Femtoseconds soliton mode-locked erbium-doped fiber laser based on nickel oxide nanoparticle saturable absorber

A. Nady[1,2], M. H. M. Ahmed[3], A. A. Latiff[4], C. H. Raymond Ooi[1], and S. W. Harun[3,*]

[1]*Department of Physics, Faculty of Science, University of Malaya, Kuala Lumpur 50603, Malaysia*
[2]*Physics Department, Faculty of Science, Beni Suef University, Beni Suef 62511, Egypt*
[3]*Department of Electrical Engineering, Faculty of Engineering, University of Malaya, Kuala Lumpur 50603, Malaysia*
[4]*Faculty of Electronic and Computer Engineering, Universiti Teknikal Malaysia Melaka, Hang Tuah Jaya 76100, Melaka, Malaysia*
**Corresponding author: swharun@um.edu.my*

Received March 19, 2017; accepted June 16, 2017; posted online July 6, 2017

We demonstrate a femtosecond mode-locked erbium-doped fiber laser (EDFL) using a nickel oxide (NiO) as a saturable absorber (SA). NiO nanoparticles are hosted into polyethylene oxide film and attached to fiber ferrule in the laser cavity. The NiO-SA shows a 39% modulation depth with a 0.04 MW/cm^2 saturation intensity. Our ring laser cavity based on erbium-doped active fiber with managed intracavity dispersion has the ability to generate ultrashort pulses with a full width at half-maximum (FWHM) of around 2.85 nm centered at 1561.8 nm. The pulses repeat at a frequency of 0.96 MHz and duration of 950 fs.

OCIS codes: 060.3510, 140.4050, 140.3510, 310.6845.
doi: 10.3788/COL201715.100602.

Mode-locked fiber lasers are among the best excellent sources for generating ultrashort optical pulses. They have a keen interest in scientific research due to their potential advantages over other types of lasers including system robustness, excellent beam quality, low cost, and reduced thermal effects. They offer a variety of applications in different fields such as optical communication, precise optical metrology, material processing, and biomedical diagnostics[1–3].

Compared to the technique of active mode locking[4,5], which requires costly bulk modulators, the passive mode-locking technique offers some potential advantages including compactness, simplicity, flexibility, and low cost. The pulses are generated passively through the internal structure of the laser cavity that gives more advantages to the output pulse signal. The most broadly used technique employs intracavity elements that allow the self-starting of the mode-locked lasing. These materials are called saturable absorbers (SAs) and are the key factor in pulsed lasers as they are able to generatepulses in one of two typical regimes, Q-switching or mode locking. SA is a nonlinear optical modulator that exhibits intensity dependent absorption in which the optical pulse itself controls its modulation depth, and the absorption coefficient decreases when the light intensity increases. SAs could be real[6] or artificial (devices that exploit the nonlinear effects to mimic the real SA action), as in mode locking based on the nonlinear polarization evolution technique[7,8].

Among the systems that can be used as real SAs, we found that the semiconductor SA mirrors (SESAMs)[9], and graphene and carbon nanotubes (CNTs) are among the widely proposed and demonstrated SAs due to their broadband saturable absorption and ultrashort recovery time[10–12]. However, the absence of a bandgap in graphene that enables broadband operation could restrain some of its applications when strong light-matter interaction is essential. Other SA materials like graphene are transition metal dichalcogenides (TMDs), such as molybdenum disulfide (MoS_2)[13,14] and tungsten disulfide (WS_2)[15,16]. Recently, topological insulators (TIs)[17,18] and black phosphorous (BP)[19,20] have been extensively investigated and demonstrated as SAs. All these materials show distinct, yet complementary, properties but the fabrication process of such SAs is complicated and costly.

In 2016, transition metal oxide nanoparticles such as zinc oxide (ZnO) and titanium dioxide (TiO_2)[21–23] have been demonstrated as SAs in a Q-switched fiber laser with results comparable to the conventional material used as an SA. A nickel oxide nanoparticle can be an effective SA as it has an appropriate modulation depth and low saturation intensity. Moreover, using the Z-scan technique on NiO films reveals nonlinear optical properties known as saturable absorption and two-photon absorption[24,25]. The absorption of photon energy for NiO has been intensively studied[26–30], and its bandgap energy was reported as 3.6–4.0 eV[31]. Therefore, the optical transition in NiO happens only through the direct interband transition. Also, NiO-SA has a very simple synthesis method and low cost.

In this Letter, we introduce a femtosecond mode-locked erbium-doped fiber laser (EDFL) by using an NiO film as an SA. The NiO-based SA is hosted into polyethylene oxide (PEO) film, which is then sandwiched between two fiber ferrules and incorporated into the laser cavity.

Nickel chloride hexahydrate and sodium hydroxide were used in the synthesis process. This synthesis was carried out by mixing the chemicals through the sonication process. In this process, at first, 1 mol/L nickel chloride hexahydrate was dissolved in 50 mL deionized water with constant stirring for 10 min. The earlier-prepared 2 mol/L solution of sodium hydroxide was then poured dropwise into the nickel chloride hexahydrate solution. The mixture was subjected to sonication using a horn sonicator. The nickel hydroxide product was collected via centrifugation and washed using deionized water. It was then calcinated at 250°C for 3 h in an electric box furnace to oxidize the nickel hydroxide to NiO nanoparticles.

The synthesized NiO nanoparticles were mixed with a PEO solution to fabricate a thin film. The thin film was developed using the solution casting technique. About 1 g of PEO was dissolved in 120 mL of deionized water and put under constant stirring for 2 h at 50°C to get a uniform solution. Then, an appropriate amount of synthesized NiO nanoparticles was added to the above solution and kept under stirring for further 2 h. The uniformly mixed slurry was cast on a Teflon Petri dish and dried at 60°C in a vacuum oven. The NiO film thickness was measured to be 0.18 ± 0.002 mm by using micrometer screw gauge.

In view of identifying the fabricated material structure, we have performed x-ray diffraction (XRD), and it shows three diffraction peaks at 37.28°, 43.28°, and 62.88° attributed to the (111), (200), and (220) planes, respectively, as shown in Fig. 1(a). The detected peaks correspond to those of nickel oxide. Figure 1(b) views the field emission scanning electron microscopy (FESEM) image showing the flake-like morphology with a particle size less than 50 nm. Figure 1(c) shows the image of the fabricated thin film. The 1 mm × 1 mm film was sandwiched between two fiber ferrules via a fiber connector with the help of index matching gel to construct a fiber-compatible SA device. The insertion loss of the device is measured to be less than 1 dB. In addition, the beam waist at the absorber is about ~10 μm, which is similar to the fiber core diameter used in the cavity.

To investigate the performance of the NiO film as an SA, the nonlinear optical response was measured by using a twin-detector technique. The measurement setup is shown in Fig. 2. In this experiment, a homemade mode-locked EDFL with a repetition frequency of 1 MHz centered at 1560 nm with a pulse duration of 2.14 ps was used as the laser source. The output pulse train from the laser was then amplified by an optical amplifier, which was connected to an optical attenuator. The signal was split equally into two; one part was a reference and connected to a power meter, and the other one passed through the SA device. The transmission characteristic of the SA film was investigated at various input signal powers, which were obtained by controlling an attenuator.

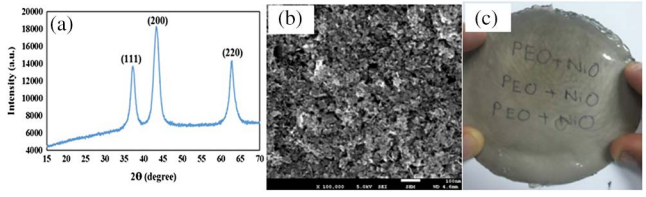

Fig. 1. Material characterization of NiO nanoparticles: (a) the XRD pattern, (b) the FESEM, and (c) the NiO-SA thin film image.

The nonlinear optical response of the SA film at different input signal intensities is recorded and plotted in Fig. 3. To measure the modulation depth, the curve obtained was then fitted using the saturation model formula[32]

$$T(I) = 1 - q_0 \times \exp\left(-\frac{I}{I_{\text{sat}}}\right) - q_{\text{ns}}, \tag{1}$$

where $T(I)$ is the transmission, q_0 is the SA modulation depth that represents the maximum change in absorption, I is the input intensity, I_{sat} is the SA saturation intensity (the intensity required to decrease the absorption to one-half of its unbleached value), and q_{ns} is the nonsaturable absorption (the loss that cannot be saturated and highly affected by the fabrication process). We found that the NiO SA film has a saturation intensity and modulation depth of 0.04 MW/cm^2 and 39%, respectively, with a nonsaturable absorption of 49%. Less surface defects such as wrinkles resulted in a low saturation intensity and increased the modulation depth[33]. Such a high modulation depth supports the strong shortening of the pulse where the pulse duration is inversely proportional to the modulation depth q_0 according to the formula[34]

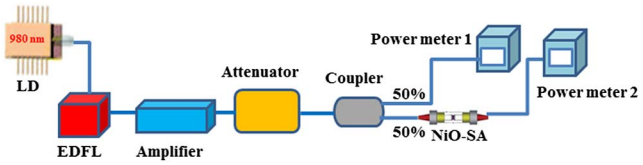

Fig. 2. Modulation depth measurement setup.

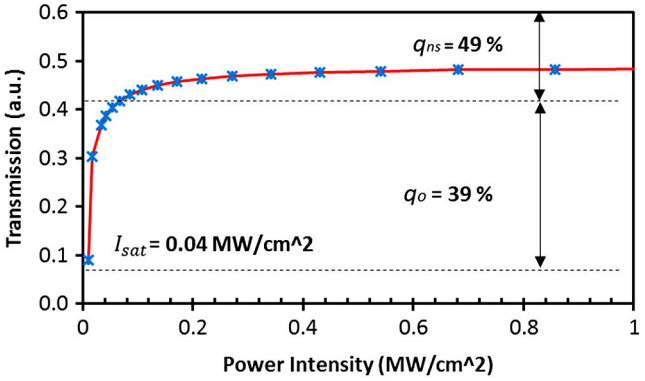

Fig. 3. Nonlinear optical absorption characteristics of the NiO-SA.

$$t_p \propto \frac{1}{q_0^s}, \tag{2}$$

where t_p is the pulse duration and q_0^s is the exponential factor that is constantly greater than 1 and varies in the different mode-locking theories.

The schematic configuration of our EDFL system with an NiO SA is shown in Fig. 4. The NiO film used as an SA can sustain damage at more than 170 mW pump power level. The pump source is a laser diode (LD) with emission centered at a wavelength of 980 nm. A piece of 3 m erbium-doped fiber (EDF) (Moritex PureCore MSFER123) was used as the lasing medium, with an absorption coefficient of 23 dB/m at 980 nm and a numerical aperture of 0.16. The EDF was core pumped by the LD through a wavelength division multiplexer (WDM). We used a polarization-insensitive isolator to guarantee unidirectional propagation of light in the laser cavity and suppress the Brillouin backscattering, which induces the pulse instability. An output coupler was used to extract only 1% from the laser. Apart from the active fiber and WDM, the rest of the fiber in the cavity is SMF-28 fiber. The total cavity length is around 208 m after adding a 200 m long SMF-28 fiber. The group velocity dispersions of the EDF and SMF-28 fiber at 1560 nm are approximately 27.6 and -21.7 ps^2/km, respectively. Also, the group velocity dispersion of 0.5 m HI1060 WDM is -48.5 ps^2/km. The net cavity dispersion was estimated to be -4.37 ps^2. The intracavity loss of the cavity is high due to an additional 200 m long SMF-28 fiber. In generating soliton mode-locking operation, more power is required to maintain oscillations in the cavity. Therefore, we used a 99% port to be oscillated back into the cavity. The output laser performance was observed using an optical spectrum analyzer (OSA) with a spectral resolution of 0.07 nm and a 350 MHz digital oscilloscope via a 1.2 GHz photodetector. We used a femtosecond autocorrelator to measure the output pulse duration. With this configuration, we only manage to generate mode-locking operation. The Q-switching operation can be realized by removing the 200 m long SMF-28 fiber.

The mode-locking operation of the laser was started at 98 mW pump power and became stable at around 100 mW pump power. Figure 5 shows the typical optical spectrum with a spectral resolution of 0.07 nm for the generated mode-locked pulses at a pump power of 165 mW. The spectrum is centered at a wavelength of 1561.8 nm with a 3 dB spectral width of about 2.85 nm showing the generated pulse operated in a soliton regime corresponding to the anomalous dispersion in the cavity. A soliton fiber laser has a pulse duration of a few ps, but for more shorter pulse durations the soliton periods become very short and the pulse becomes unstable because of very high nonlinear phase shifts per round trip where the nonlinear phase shift per cavity round trip is inversely proportional to the pulse duration. In the proposed EDFL, the pulse spectrum shows Kelly sidebands as observed in our spectrum where our pulse duration is very short (950 fs).

The temporal profile of the mode-locked EDFL has also been investigated by using an autocorrelator and oscilloscope. The oscilloscope trace views a stable pulse train as shown in Fig. 6(a). As shown in the figure, two adjacent pulses are separated by 1.04 μs, which corresponds to a 0.96 MHz repetition rate. The obtained pulse duration of 0.043 μs is not the actual value because of the resolution limitation in the oscilloscope. Thus, the pulse duration was measured using an optical autocorrelator and mathematically calculated using the time-bandwidth product (TBP) formula. Figure 6(b) indicates the measured autocorrelator pulse trace has a sech^2 pulse profile and a full width at half-maxium (FWHM) of 950 fs with a TBP of 0.332, confirming the pulse is slightly chirped. The minimum possible pulse duration calculated mathematically is about 900 fs in in the sech^2 pulse profile.

To investigate the laser performance and pulse stability, we measured the degree of suppression of the adjacent harmonics or side modes through the radio frequency (RF) spectrum, as shown in Fig. 7(a). It indicates that the fundamental frequency of our fiber laser cavity is 0.96 MHz and the side modes are suppressed by about 43 dB, confirming the stability of the pulse. This film has been tested by continuously running the laser for 48 h, and yet the mode-locking performance was still unchanged. Compared to graphene, NiO has a higher modulation depth.

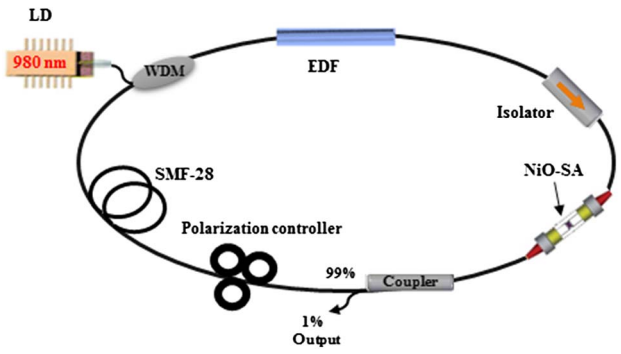

Fig. 4. Schematic diagram of the experimental setup.

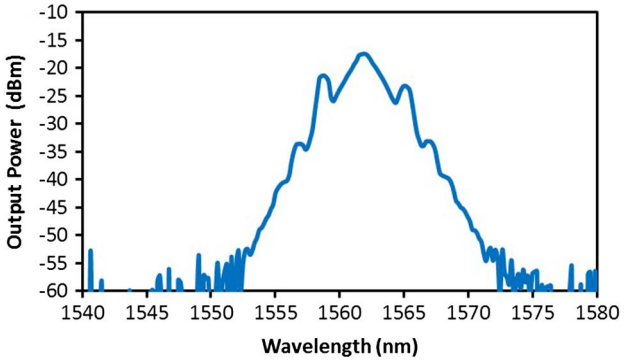

Fig. 5. Output spectrum of the mode-locked EDFL at a pump power of 165 mW.

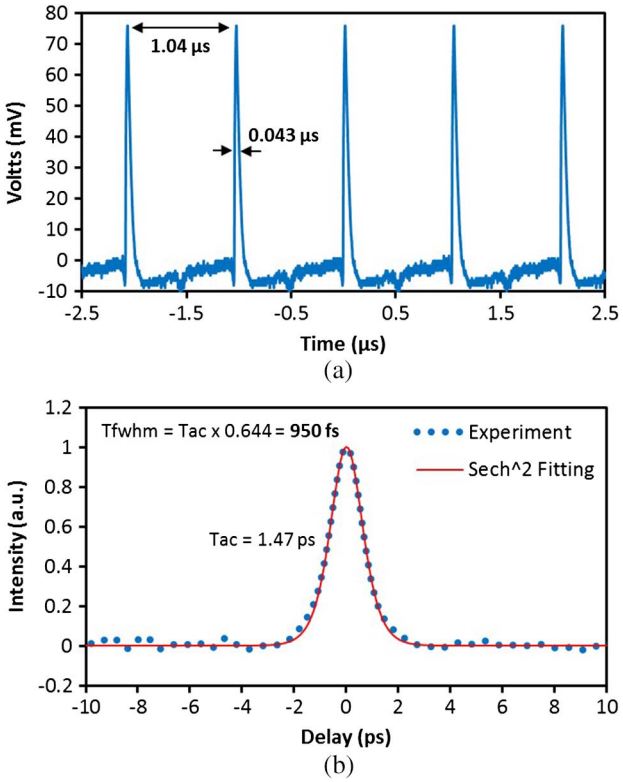

Fig. 6. (a) Oscilloscope train at a pump power of 165 mW. (b) The autocorrelation trace.

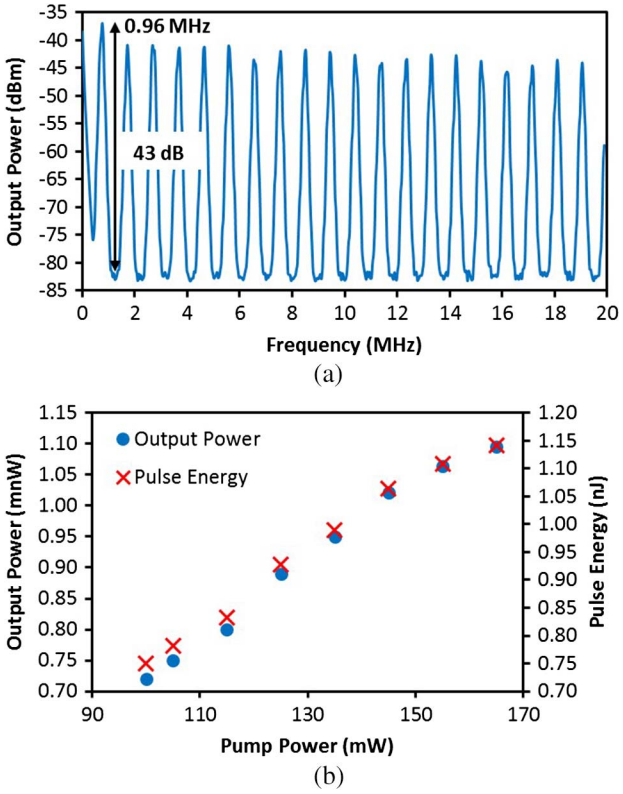

Fig. 7. (a) RF spectrum with 20 MHz span. (b) The output power and pulse energy.

Figure 7(a) shows the output power and pulse energy of the mode-locked laser versus the pumping power. The output power increases from 0.72 to 1.09 mW as the pump power is raised from 100 to 165 mW. The pulse energy is also increased with increasing pump power, and it has a considerable value; for example, we obtained a pulse energy of 1.14 nJ at a pump power of 165 mW, although the output pulse laser was obtained through a 99/1 output coupler. The higher pulse energy can be achieved by improving the intracavity losses or reducing the repetition rate (increasing the cavity length). In our result, we successfully produce a short pulse width a size of 950 fs, which becomes the main contribution to the high peak power of 1.2 kW.

We successfully demonstrate an ultrashort mode-locked EDFL in a ring cavity using an NiO-based SA whose fabrication process is simple and low cost. The generated optical pulses have an FWHM of about 2.85 nm centered at 1561.8 nm, with a considerable energy of 1.14 nJ at a 165 mW pump power, although the output pulse laser is obtained through a 99/1 output coupler. The pulses have a duration of 950 fs with a repetition frequency of 0.96 MHz. The results affirm that NiO can be used as an effective SA in mode-locked fiber lasers and serve in ultrafast photonic applications.

References

1. X. Liu, Y. Cui, D. Han, X. Yao, and Z. Sun, Sci. Rep. **5**, 9101 (2015).
2. U. Keller, Nature **424**, 831 (2003).
3. B. Oktem, C. Ülgüdür, and F. Ö. Ilday, Nat. Photon. **4**, 307 (2010).
4. M.-Y. Jeon, H. K. Lee, K. H. Kim, E.-H. Lee, W.-Y. Oh, B. Y. Kim, H.-W. Lee, and Y. W. Koh, Opt. Commun. **149**, 312 (1998).
5. Y. M. Chang, J. Lee, and J. H. Lee, Jpn. J. Appl. Phys. **51**, 072701 (2012).
6. R. I. Woodward and E. J. Kelleher, Appl. Sci. **5**, 1440 (2015).
7. M. Fermann, M. Stock, M. Andrejco, and Y. Silberberg, Opt. Lett. **18**, 894 (1993).
8. M. Nikodem and K. Abramski, Opt. Commun. **283**, 109 (2010).
9. H. Zhang, D. Tang, L. Zhao, and N. Xiang, Opt. Express **16**, 12618 (2008).
10. H. Zhang, D. Y. Tang, L. M. Zhao, Q. L. Bao, and K. P. Loh, Opt. Express **17**, 17630 (2009).
11. A. Martinez, K. Fuse, and S. Yamashita, Appl. Phys. Lett. **99**, 121107 (2011).
12. S. Y. Set, H. Yaguchi, Y. Tanaka, and M. Jablonski, IEEE J. Sel. Top. Quantum Electron. **10**, 137 (2004).
13. J. Du, Q. Wang, G. Jiang, C. Xu, C. Zhao, Y. Xiang, Y. Chen, S. Wen, and H. Zhang, Sci. Rep. **4**, 6346 (2014).
14. H. Liu, A.-P. Luo, F.-Z. Wang, R. Tang, M. Liu, Z.-C. Luo, W.-C. Xu, C.-J. Zhao, and H. Zhang, Opt. Lett. **39**, 4591 (2014).
15. P. Yan, A. Liu, Y. Chen, J. Wang, S. Ruan, H. Chen, and J. Ding, Sci. Rep. **5**, 12587 (2015).
16. P. Yan, A. Liu, Y. Chen, H. Chen, S. Ruan, C. Guo, S. Chen, I. L. Li, H. Yang, and J. Hu, Opt. Mater. Express **5**, 479 (2015).
17. C. Zhao, H. Zhang, X. Qi, Y. Chen, Z. Wang, S. Wen, and D. Tang, Appl. Phys. Lett. **101**, 211106 (2012).
18. J. Lee, J. Koo, Y. M. Jhon, and J. H. Lee, Opt. Express **22**, 6165 (2014).
19. Y. Chen, G. Jiang, S. Chen, Z. Guo, X. Yu, C. Zhao, H. Zhang, Q. Bao, S. Wen, and D. Tang, Opt. Express **23**, 12823 (2015).

20. Z. C. Luo, M. Liu, Z. N. Guo, X. F. Jiang, A. P. Luo, C. J. Zhao, X. F. Yu, W. C. Xu, and H. Zhang, Opt. Express **23**, 20030 (2015).
21. H. Ahmad, C. Lee, M. Ismail, Z. Ali, S. Reduan, N. Ruslan, M. Ismail, and S. Harun, Opt. Commun. **381**, 72 (2016).
22. H. Ahmad, S. Reduan, Z. A. Ali, M. Ismail, N. Ruslan, C. Lee, R. Puteh, and S. Harun, IEEE Photon. J. **8**, 1 (2016).
23. A. Latiff, M. Rusdi, M. Hisyam, H. Ahmad, and S. Harun, J. Mod. Opt. **64**, 187 (2017).
24. S. Shablaev and R. Pisarev, Phys. Solid State **45**, 1742 (2003).
25. R. P. de Melo, Jr., B. J. da Silva, F. E. P. dos Santos, A. Azevedo, and C. B. de Araújo, J. Appl. Phys. **106**, 093517 (2009).
26. M. Utriainen, M. Kröger-Laukkanen, and L. Niinistö, J. Mater. Sci. Eng. B **54**, 98 (1998).
27. A. Šurca, B. Orel, B. Pihlar, and P. Bukovec, J. Electroanal. Chem. **408**, 83 (1996).
28. Y. Xie, W. Wang, Y. Qian, L. Yang, and Z. Chen, J. Cryst. Growth **167**, 656 (1996).
29. R. Misho, W. Murad, G. Fatahalah, I. Aziz, and H. Al-Doori, Phys. Status Solidi A **109**, K101 (1988).
30. A. Varkey and A. Fort, Thin Solid Films **235**, 47 (1993).
31. J. Wang, P. Yang, X. Wei, and Z. Zhou, Nanoscale Res. Lett. **10**, 1 (2015).
32. Z. Tian, K. Wu, L. Kong, N. Yang, Y. Wang, R. Chen, W. Hu, J. Xu, and Y. Tang, Laser Phys. Lett. **12**, 065104 (2015).
33. H. Zhu, L. Zhao, J. Liu, S. Xu, W. Cai, S. Jiang, L. Zheng, L. Su, and J. Xu, Opt. Eng. **55**, 081304 (2016).
34. I. Jung, F. Kärtner, N. Matuschek, D. Sutter, F. Morier-Genoud, Z. Shi, V. Scheuer, M. Tilsch, T. Tschudi, and U. Keller, Appl. Phys. B **65**, 137 (1997).